International Journal of Bifurcation and Chaos, Vol. 33, No. 11 (2023) 2350130 (18 pages)

DOI: 10.1142/S0218127423501304

Fuzzy Sampled-Data Stabilization of Hidden Oscillations in a Memristor-Based Dynamical System

T. Bhagyaraj
Periyar Maniammai Institute of Science and Technology, Vallam, Thanjavur 613 403, India
pakiarajthangavel@gmail.com

S. Sabarathinam* and Viktor Popov†
Laboratory of Complex Systems Modelling and Control, Faculty of Computer Science, National Research University, High School of Economics, Moscow 109 028, Russia
**saba.cnld@gmail.com*
†*masterlu@mail.ru*

K. Thamilmaran
Centre for Nonlinear Systems, Chennai Institute of Technology, Chennai 600 044, Tamilnadu, India
maran.cnld@gmail.com

R. Vadivel
Department of Mathematics, Faculty of Science and Technology, Phuket Rajabhat University, Phuket 83000, Thailand
vadivelsr@yahoo.com

Nallappan Gunasekaran
Eastern Michigan Joint College of Engineering, Beibu Gulf University, Qinzhou 535 011, P. R. China
gunasmaths@gmail.com

Received April 10, 2023; Revised May 28, 2023

In the manuscript, we report the dynamics of the Takagi–Sugeno (T–S) fuzzy memristor-based hidden system via sampled-data control. For an open-loop formulation, the system dynamics are studied. We found extreme events, hidden attractors, and trivial period doubling scenarios and confirmed them through numerical, analytical, statistical and experimental analyses. Furthermore, to enable stability analysis and control combination, the (T–S) fuzzy algorithm is employed to control the dynamics of a nonlinear system. First, we designed the sampled data fuzzy controller (SDFC) for the proposed system. Second, the Lyapunov–Krasovskii functional (LKF) strategy, novel integral inequality mechanisms, and certain sufficient conditions are determined by deriving the linear matrix inequalities (LMIs), which ensure the asymptotic stability of the system. Moreover, the sampled data control gains are computed for the large sampling interval, and numerically obtained results confirm the theoretical results. Additionally, a simple

*Author for correspondence

real-time analog electronic circuit is constructed, and experimental data is obtained, and finally, numerically simulated results were verified through MATLAB.

Keywords: Memristor; hidden attractor; extreme event; linear matrix inequality; sampled-data control; T–S fuzzy system.

1. Introduction

The idea of *memristors* is a timely contribution to the field of circuit systems, and it benefits science and technology due to its potential applications [Shin *et al.*, 2010; Kim *et al.*, 2012; Gunasekaran *et al.*, 2021a]. The memristor was introduced [Chua, 1971] as a new fourth passive circuit element that relates charge (q) and flux (ϕ) and has received too much attention in circuit theory [Jothimurugan *et al.*, 2017; Sabarathinam & Thamilmaran, 2017; Varshney *et al.*, 2018b]. It has broad applications from science to the technological world because of its nonvolatile memory property. The concept of the memristor is applied in a variety of fields such as neuromorphic computing [Burr *et al.*, 2017], digital circuits, logic circuits, biological and neuromorphic systems, computer technology, and digital as well as analog memory. Therefore, understanding the memristor property is of great importance. The construction of a memristor was examined by HP Labs, leading to the discovery of some prototype memristor elements [Hamdioui *et al.*, 2013]. Using the theory of memristor in complex systems, researchers have been inspired to study memristor-based dynamical systems in recent years, incorporating different forms of memristor nonlinearity such as piecewise linear (PWL) [Swathy *et al.*, 2014], cubic [Thangavel *et al.*, 2021; Sabarathinam & Prasad, 2018] and Tanh [Ueta *et al.*, 2004] nonlinearity. These memristor-formulated dynamical systems provide more insight into understanding the construction of memristor components. The advantage here is that a memristor-based complex system could contain hidden oscillations as well as extreme events. These results are important to know for the construction of memristor emulators in the above-mentioned variety of applicable fields. Moreover, extreme events (EEs) are usually believed to be commonly rare and unexpected events and/or events that deviate extremely from normalcy. EEs are very rare events that have recently been reported and investigated in natural and man-made systems such as floods [Kirezci *et al.*, 2020], rogue waves [Knobler *et al.*, 2021], tsunamis [Meilianda *et al.*, 2021], earthquakes [Poblete *et al.*, 2018], and predatory populations [Chaurasia *et al.*, 2020]. Recently, researchers have identified a few mechanisms and ways through which EEs occur, such as interior crises [Mishra *et al.*, 2020; Thangavel *et al.*, 2022], boundary crises [Osinga & Feudel, 2000], discontinuous boundaries [Kumarasamy & Pisarchik, 2018] and very recently an intermittent route [Premraj *et al.*, 2021] through complex system studies.

In addition, the *hidden attractor* (a basin of attraction that does not intersect with the unstable fixed point) and its dynamics are intriguing phenomena that have been studied considerably over recent years in diverse fields [Kiseleva *et al.*, 2016; Andrievsky *et al.*, 2016; Kuznetsov *et al.*, 2015]. Especially, hidden attractors were identified in dynamical systems [Dudkowski *et al.*, 2016; Jafari *et al.*, 2015; Danca, 2021], fractional systems [Liu *et al.*, 2021], memristor systems [Saha *et al.*, 2015] and multistable systems [Jafari *et al.*, 2018]. Some results have been devoted to studying the occurrence of hidden attractors in electronic circuits [Hu *et al.*, 2016; Pham *et al.*, 2018]. In this context, controlling the dynamics of hidden attractors using linear augmentation has been reported in [Sharma *et al.*, 2015].

The existence of extreme events in a hidden-based system is a lacuna. Even though, there are no such investigations in the memristor-based hidden oscillatory systems to investigate the extreme events. Based on the foregoing motives, we investigated hidden attractors and extreme events in a memristor-based dynamical system for the first time in this work. The current study contributes to a better understanding of memristor nonlinearity and the discovery of hidden dynamics. By matching with numerical results, the resulting experimental data guarantee the hidden attractors and extreme events. We build the memristor system using the cubic form [Thangavel *et al.*, 2021] of memristor nonlinearity.

The second phase of the manuscript aims to control the dynamics of the proposed model using a

sampled-data control (SDC) approach. The Takagi–Sugeno (T–S) fuzzy model has been widely used to effectively approximate the nonlinear systems [Wang *et al.*, 2019; Vadivel *et al.*, 2022; Li *et al.*, 2020; Gunasekaran *et al.*, 2021b; Thangavel *et al.*, 2022]. The scope of SDC research has prolonged to addressing the stabilization issue of the T–S fuzzy model, which can represent a wide range of nonlinear systems by utilizing a weighted average of linear models. With amazing improvements in digitalized technology, the applications of control sectors such as automobile control, industrial machinery control, and electric grid control have quickly undergone digitalization [Vadivel *et al.*, 2021; Ding & Zhu, 2020; Gunasekaran *et al.*, 2021a; Ackermann, 2012; Wang *et al.*, 2019; Gunasekaran *et al.*, 2021b; Anbuvithya *et al.*, 2021; Ackermann, 2012]. There has been a rise in the importance of SDC in embedded systems that use digital control modules. The reason for such embedded systems that execute several jobs must lower their operating burden practically concurrently by reducing the quantity of sent signals based on a sample interval threshold determined by the SDC method. Notably, the SDC has the broadest range of applications compared to other controllers. Furthermore, each controller is subject to its own set of limitations, and the SDC is no exception. Therefore, the SDC has received a lot of attention in current research [Gunasekaran & Joo, 2019]. In [Shi *et al.*, 2020], studied switched fuzzy SDC, nonfragile filtering of T–S fuzzy NNs. In [Shanmugam & Joo, 2020] and [Sakthivel *et al.*, 2023], SDC was designed and analyzed through a large-scale interconnected power system and fractional-order memristive NNs. Moreover, the linear matrix inequalities (LMIs) tool is a powerful strategy for dealing with practical systems to find the stability and stabilization properties [Zhai & Xu, 2011]. The study of system stability through the use of SDC has garnered significant interest and presents promising research opportunities in the long term. As far as the author is aware, there are currently no published results on the development of fuzzy sampled-data stabilization techniques for memristor-based hidden dynamical systems. This serves as one of the key motivations for writing this note.

Recently, the Takagi–Sugeno (T–S) fuzzy model has been widely used to effectively approximate the nonlinear systems in [Vadivel *et al.*, 2021; Gunasekaran *et al.*, 2021b], and the (T–S) fuzzy controller has also been successfully applied to stability control design of nonlinear systems. To avoid solving the vexing Hamilton–Jacobi inequality, the (T–S) fuzzy inference system is often used to approximate the nonlinear financial systems, which are several local linear financial systems at various operating points. On the other hand, in financial systems, supervision, and sampled-data control can be viewed as a way to design a manageable strategy to minimize the investment risk due to inherent continuous and discontinuous random fluctuations. Moreover, the sampled-data control strategy needs to solve the difficulty of Hamilton–Jacobi inequality to achieve the required nonlinear financial systems steady by the state (target). In some practical implementations, it is very difficult to guarantee that the signals will be transmitted continuously. Digital controllers tend to replace continuous-time controllers under digital technology and communication networks. At the same time, with the rapid development of microelectronics technology and the limitation of communication bandwidth, the control of the sampled data that only changes the signal at the sampling instant has the advantages of occupying fewer communication channels, fewer transmission of signals, and low cost [Anbuvithya *et al.*, 2021]. Therefore, the sampled-data control (SDC) has received a lot of attention in current research [Gunasekaran & Joo, 2019].

Motivated by the preceding research, this study aims to develop a Fuzzy Sampled-Data Stabilization approach for memristor-based hidden dynamical systems, expanding on previous investigations. The following are the most significant contributions of this work:

- The memristor-based hidden system has been constructed for the first time in laboratory real-time hardware experiments.
- The mechanism underlying the extreme events was established, and the hidden attractors were investigated.
- The controlling tactics are used, and similarities with the limited basin structure are drawn for the first time.
- The suggested method entails building a standard Lyapunov–Krasovskii functional (LKF) and deriving the appropriate stabilization conditions using linear matrix inequalities (LMIs) and integral inequality techniques. The effectiveness of this strategy is proven by illustrative examples.

The following describes the way the manuscript is structured. Section 2 discusses the formation of the memristor concept, along with stability analysis and the physical situation with respect to the initial conditions of the memristive hidden attractor system. Section 3 covers numerical results such as confirming the presence of extreme events and hidden attractors. Section 4 describes how to control extreme events in a memristive hidden system utilizing the Takagi–Sugeno (T–S) fuzzy model formulation. Section 5 provides the experimental realization, circuit equations, and results. Section 6 summarizes the simulation results. Finally, in Sec. 7, the present manuscript is concluded.

2. Memristor Formulation and System Construction

The formulation of the memristor is available in several reports in the literature [Corinto & Forti, 2016; Haghiri *et al.*, 2017; Kahale & Tannir, 2021] and in our previous articles [Varshney *et al.*, 2018b; Varshney *et al.*, 2018a]. Here, we present a short note on memristor formulation. From Ohm's law, the memristor is defined as a memory resistor instead of a classical resistor. It is defined as,

$$i = W(\phi)v, \tag{1}$$

where $W(\phi)$ is considered as memristor (nonlinear functions) called memductance. This memductance is defined as,

$$W(\phi) = \frac{dq(\phi)}{d\phi}. \tag{2}$$

The above Eq. (1) can be written as,

$$i = \frac{dq}{dt} = \frac{dq}{d\phi}, \quad \frac{d\phi}{dt} = \frac{dq}{d\phi}, \quad v = W(\phi)v. \tag{3}$$

In this paper, we have designed cubic nonlinearity-based flux-controlled memristor ($W(\phi)$) as follows,

$$q(\phi) = a\phi + b\phi^3. \tag{4}$$

In this case, the memductance is given as,

$$W(\phi) = a + 3b\phi^2, \tag{5}$$

where, $W(\phi)$ is the cubic nonlinearity form of the flux-controlled memristor. The cubic nonlinear form can be transformed into a memristor-based nonlinearity Eq. (5) which is shown in Fig. 1 [Bao *et al.*, 2017]. Nodes A and B refer to the input and output of the flux-controlled memristor. For constructing the memristor-based dynamical system, consider the following fourth-order nonlinear system [Liu *et al.*, 2020] by utilizing the memristor concept as follows,

$$\begin{cases} \dot{x} = -x + y, \\ \dot{y} = -x + yz + W(\omega)y, \\ \dot{z} = E - y^2, \\ \dot{w} = y, \end{cases} \tag{6}$$

where $W(\omega)$ represents flux controlled memristor, where $W(\omega) = a + 3bw^2$, and E is an external bias. We take the external bias as a tuning parameter to understand the system dynamics.

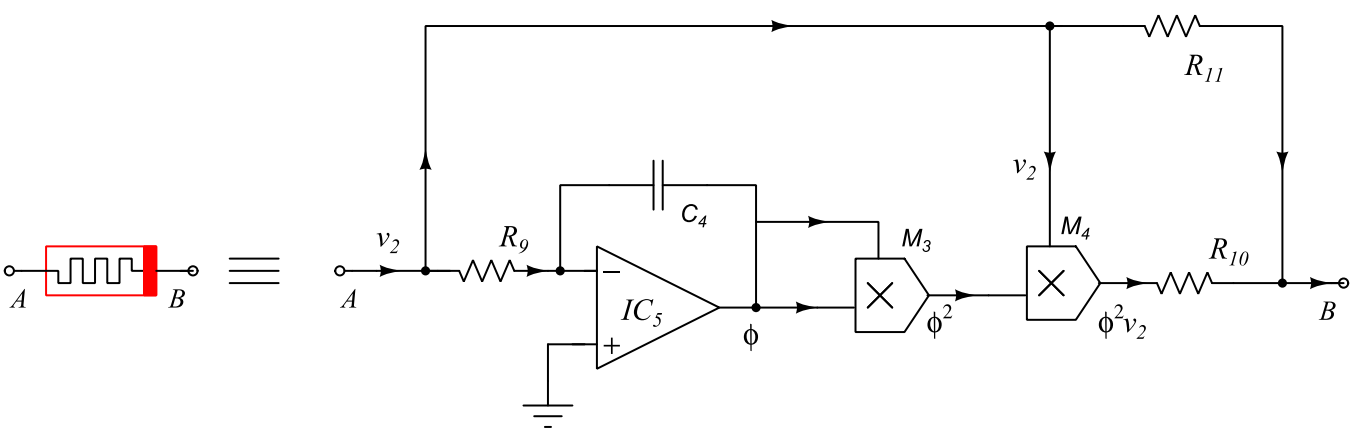

Fig. 1. Schematic circuit diagram of the flux controlled memristor [$W(\omega)$] cubic nonlinearity.

2.1. *Stability analysis*

The equilibrium point is computed initially to determine the system's stability in order to demonstrate hidden oscillations. The velocity components ($\dot{x}, \dot{y}, \dot{z}, \dot{w}$ derivatives) and the external bias "E" in the system (6) are assumed to be zero

$$\begin{cases} 0 = -x + y, \\ 0 = -x + yz + (a + 3bw^2)y, \\ 0 = E - y^2, \\ 0 = y. \end{cases} \tag{7}$$

The solution of Eq. (7) yields the system's equilibrium as $x^*, y^*, z^*, w^* = (0, 0, 0, 0)$. The Jacobean can be written as follows to yield eigenvalues:

$$J = \begin{bmatrix} -1 & 1 & 0 & 0 \\ -1 & \Delta & y & 6b\omega y \\ 0 & -2y & 0 & 0 \\ 0 & 1 & 0 & 0 \end{bmatrix}, \tag{8}$$

where, $\Delta = z + a + 3bw^2$, the system has the following type of stability.

Case 1. For $(x, y, z, w = 0)$

The eigenvalues are calculated from Eq. (8) as $\lambda_{1,4} = 0$ (*degenerate cases*), and $\lambda_{2,3} = -0.4999 \pm 0.8660i$ (*stable focus*) at the trivial equilibrium point at zero. Based on this study, wherever the initial conditions are started to simulate the system, the system will reach a fixed point. There is no possibility of attraction. However, as shown in Fig. 2, attractors do not overlap with the basin at zero and exist apart from trivial equilibrium points. These are known as "hidden attractors" [Kuznetsov *et al.*, 2015]. Case II is the following assumption, which is used to determine the explanation behind it.

Case II. The second Eq. (7), the memristor component is considered as follows,

$$\begin{aligned} &(a + 3bw^2)y = 0, \\ &y = 0, \quad (a + 3bw^2) = 0; \\ &w = \pm\sqrt{\frac{a}{3b}}. \end{aligned} \tag{9}$$

To determine the stability of this equilibrium point, $x, y, z = 0$ and $w \neq 0$, i.e. $w = \pm\sqrt{\frac{a}{3b}}$: $\lambda_{1,4} = 0$ (*degenerate cases*), and $\lambda_{2,3} = -0.4999 \pm 0.8660i$ (*stable focus*). There are no changes to the stability requirements. However, while utilizing the XPPAUTO software to draw the system's nullclines, we have the stable line of the state variable w at 0.57. The values are calculated using Eq. (9) for a and $b = 0.0001$.

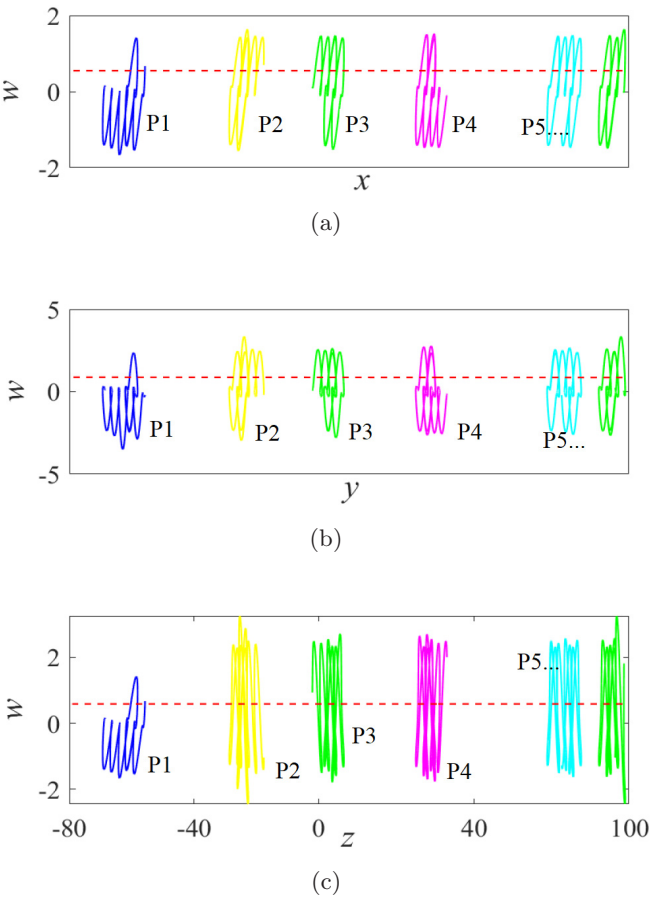

Fig. 2. Numerically computed hidden attractors in the (x–w), (y–w) and (z–w) planes. Different sets of attractors (P1, P2, P3 . . .) (chaotic at $E = 0.57$) are redrawn on the same plane.

Figure 2 depicts multiple hidden attractors that fall along the red dashed line of the w-axis. According to [Varshney *et al.*, 2018b], the w-axis has an infinite range of stable equilibrium line. This type of stability is known as *periodic line invariant* [Varshney *et al.*, 2018a]. Figure 2, depicts several periodic attractors denoted as P1, P2, P3, P4, P5 . . . that exist along the w-axis on the (x–w), (y–w), and (z–w) planes. That is, a w-axis possesses *stable focus* stability. There are no nullclines in the (w) plane, and the rest are depicted in Fig. 2. According to this stability study, the oscillation is not affected by the stability basin or the basin of attraction. This type of attractor is known as *hidden attractors*.

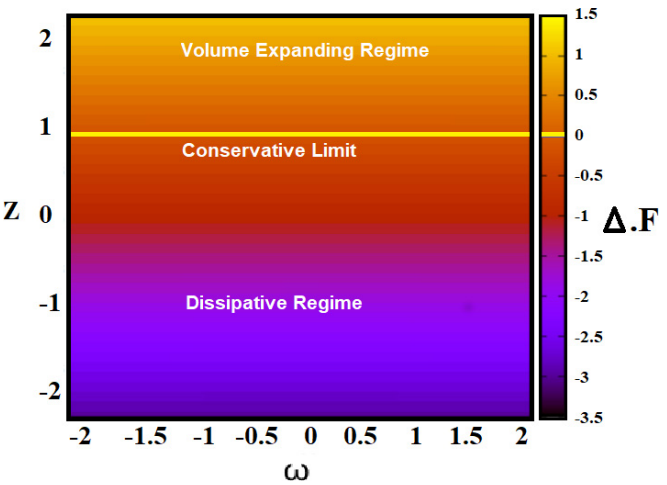

Fig. 3. Changes in the physical situation of the system (6). The initial conditions (z, w) varied in the ranges of $-2 \in 2$, and the third axis (color bar) is the volume parameter $\Delta \cdot F$.

2.2. *Physical situation*

To study the conservative/dissipativeness of the present system (6), it can be calculated as,

$$\Delta \cdot F = \frac{\partial F_1}{\partial x} + \frac{\partial F_2}{\partial y} + \frac{\partial F_3}{\partial z} + \frac{\partial F_4}{\partial w}, \tag{10}$$

$$\Delta \cdot F = -0.9999 + z + 0.0003\omega^2. \tag{11}$$

According to Eq. (11), the system transitions from a dissipative to a conservative physical state with respect to the initial conditions ω and z. Figure 3 depicts $\Delta \cdot F$ (color bar) with regard to the state variables ω and z to help comprehend the transition. The picture depicts the volume expanding $(\Delta \cdot F > 0)$ regime, the dissipative regime $(\Delta \cdot F < 0)$, and the conservative limits $(\Delta \cdot F = 0)$.

3. Numerical Results

A bifurcation and Lyapunov exponent spectrum helps in understanding the dynamics of our proposed system's local dynamics. Figure 4 depicts (a) a bifurcation diagram in the $(E$–$y)$ plane with respect to E in the range of $\in (0, 1)$ and (b) Lyapunov exponents in the $(E$–$\lambda_{1,2,3})$ plane. The hidden dynamics are summarized in the bifurcation diagram and its Lyapunov exponents as follows.

- The familiar period doubling route obtained in the range $(0 < E \leq 0.362)$.
- The chaotic regimes exist in wide ranges of $(0.386 < E \leq 0.63)$, followed by a few periodic windows it appear.
- The extreme events were obtained in the parameter range of $(0.635 < E \leq 0.685)$.

The extreme event values of visualizing phase portraits and time series in Fig. 5 are taken from the bifurcation plot, as indicated by the red vertical dashed line in Fig. 4.

3.1. *Extreme event*

For visualizing the EEs in phase space, if we fix external biasing at $E = 0.625$, chaotic attractor exists. Further increasing the bias, this chaotic attractor has large amplitude pulses. The pulses are crossed over the EE thresholds i.e. extreme events (EEs). Figure 5 shows chaotic and EEs of (i) phase portraits and (ii) time series. The extreme events threshold is defined in the literature as, $\text{EE} = \mu + n\sigma$, where μ, σ is the mean and standard deviations of the data set and the integer n defines EEs in the range of $(4 < n \leq 8)$. Here, EEs threshold is obtained as $\text{EE} = 4.0458$ by considering $n = 6$.

The three-dimensional phase portraits are drawn as shown in Fig. 6 to differentiate the (a) chaos (CH), and (b) extreme events (EEs). From this three-dimensional visualization the chaos and extreme events are clearly visualized.

3.2. *Phase slips analysis*

Very few measures were reported in the literature to confirm the presence of extreme events.

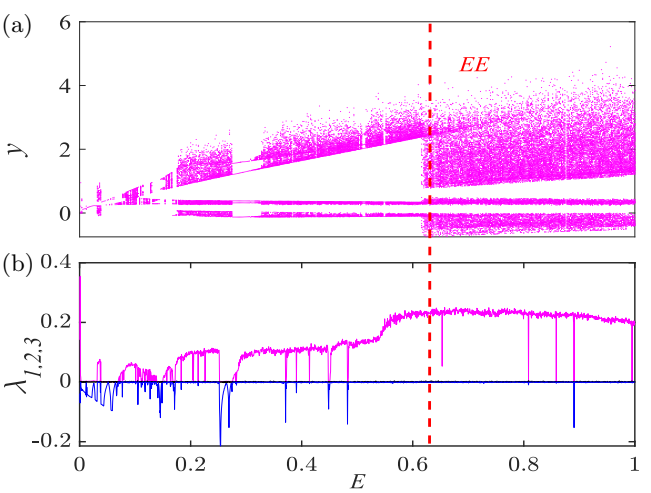

Fig. 4. Numerically computed, (a) bifurcation diagram in the $(E$–$y)$ plane with respect to external self-feedback E in the range of $\in (0, 1)$ and its corresponding and (b) Lyapunov exponents in the $(E$–$\lambda_{1,2,3})$ plane.

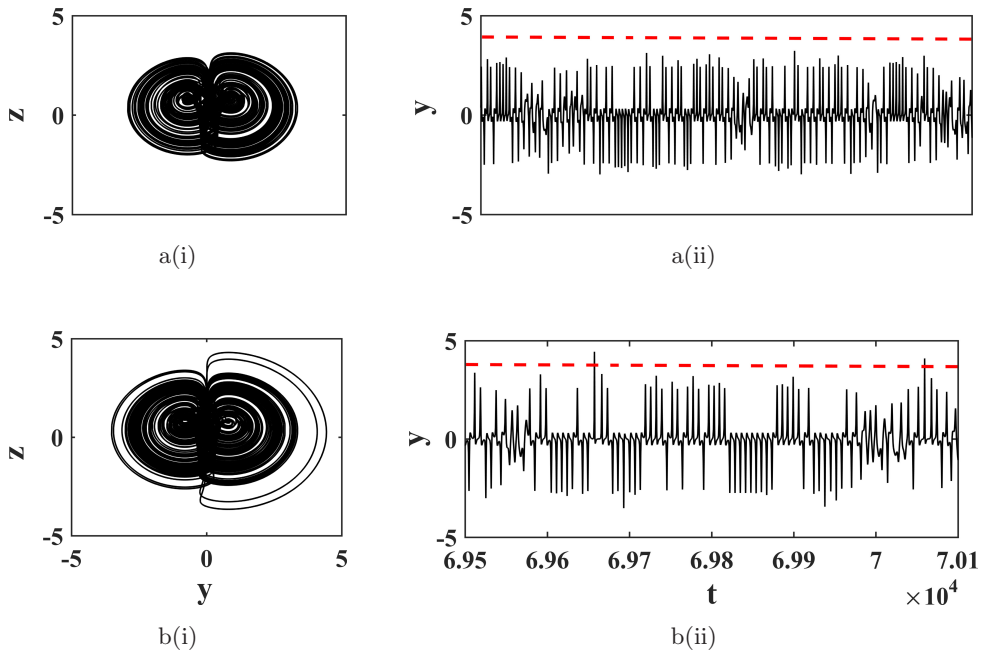

Fig. 5. Numerically obtained typical (i) phase portraits in the (y–z) plane and (ii) time series of $y(t)$. (a) Chaotic attractor at $E = 0.625$ and (b) extreme event at $E = 0.6545$. The horizontal dashed red color line shows the EEs threshold value of $n = 6$.

The measurement of phase slips is one of the best tests for determining the presence of extreme events (EEs). The Hilbert transform is used to calculate the instantaneous phase (ϕ) of the considered signals of (EEs). The phase differences between the original signal (EE) and its corresponding Hilbert-transformed signal are then calculated ($\delta\phi = \phi y(t) \approx \phi H(u)t$). Take note that the phase difference is complete in terms of the system's time evolution. Because of the randomness of chaotic oscillations, the phase is continuously increasing with respect to time in phase slips analysis; similarly, an instantaneous phase is consistent with respect to time in periodic oscillations.

In the case of extreme events, the instantaneous phase extends in the chaotic regime and it abruptly gets slipped in multiples of π during the occurrence of EEs. Notice that some basin threshold is sustained depending on basin size, whenever the trajectories flee from the threshold basin then phase slips occurred. In our present study, we specified the threshold basin as $\pm\pi$. These are shown in Figs. 7(a)

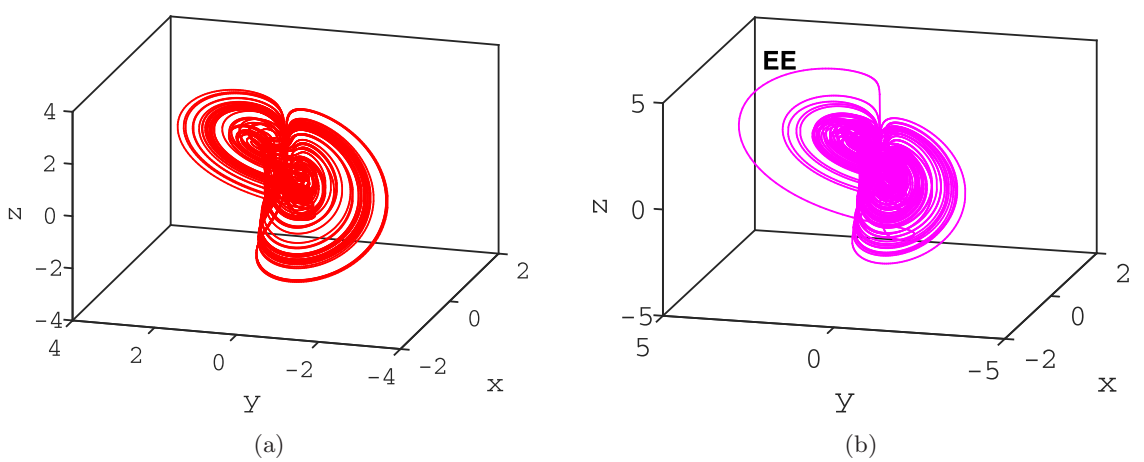

Fig. 6. Three-dimensional phase portraits of the coexistence of phase trajectories. (a) Chaotic oscillation and (b) extreme events (EEs) oscillation.

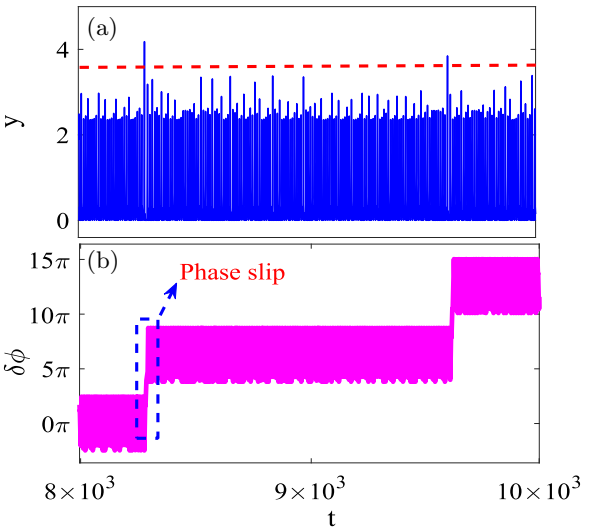

Fig. 7. Numerically obtained (a) time series of EEs of $y(t)$ state variable and (b) $(\delta\phi)$ calculation. EEs threshold is mentioned horizontally in red dashed lines and phase slips are also mentioned in blue color rectangle dashed lines.

and 7(b), wherein phase slips $(\delta\phi)$ are plotted as a function of time t extreme event regime $E = 0.6545$.

3.3. *Probability distribution function*

Furthermore, we were able to confirm EEs using a simple probability distribution (PDF) measurement. The EEs regime was identified with a small sub-distribution in the tail of the original PDF distribution regime for this calculation. The state variable $y(t)$ with extreme events incorporating time series was considered for PDF estimation. Figure 8 illustrates the PDF as a function of state variable amplitude $y(t)$ taken as 5×10^7 data points. The predominant chaotic regime is shown in fine Gaussian distribution in the figure in the ranges of

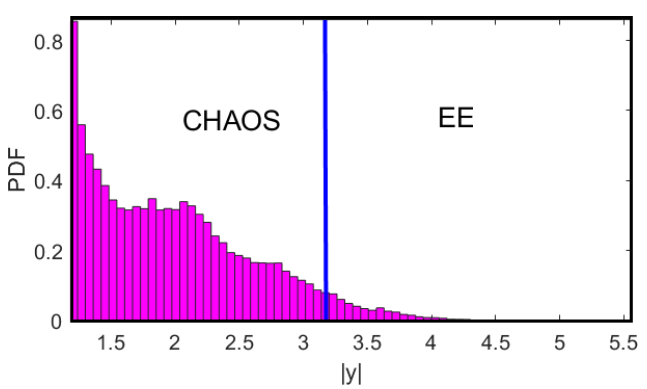

Fig. 8. Numerically computed probability distribution function (PDF) of EE time series at $E = 0.6545$.

$|y| \in [0, 3.2]$. The portion of extreme events pinpointed in tail portion $|y| \in [3.2, 4.5]$ seen as a blue colored vertical line is the classified EE's prominence of calculated time series. Notice that here, we present the zoomed portion of PDF starting from $y(t) \in [1.2, 5.5]$. But the mean of time series starts from zero itself. We have demonstrated the portion of EE and chaos in the same time scale. For that we present the portion of the PDF.

4. Controlling Sections

In this section, we introduce controlling terms or control inputs in system (6) and consider the following stabilization of the system

$$\begin{cases} \dot{x} = -x + y + u_1(t), \\ \dot{y} = -x + yz + W(\omega)y + u_2(t), \\ \dot{z} = E - y^2 + u_3(t), \\ \dot{w} = y + u_4(t), \end{cases} \tag{12}$$

where $u_1(t)$, $u_2(t)$, $u_3(t)$ and $u_4(t)$ are control inputs and $W(\omega)$ is the independent value.

It is important to point out that the solution displays a fluctuating behavior, with the variable, y, alternating between positive and negative values in an unpredictably chaotic way. This behavior is something that should be noted. The chart of $y(t)$ versus time, t, seems like random vibrations despite the fact that the circumstances have a deterministic quality to them and that the beginning conditions can be controlled. The frequency and amplitude of the oscillations, however, do not change throughout the course of time, demonstrating that the system does exhibit some degree of regularity. Given that we are working with the assumption that $y(t) \in [-2, 2]$ we are able to create a fuzzy model for any range of $y(t)$.

Defining $X(t) = y(t)$ for the nonlinear term, (12) can be described as

$$\dot{X}(t) = \begin{bmatrix} -1 & 1 & 0 & 0 \\ -1 & W(w) & X & 0 \\ 0 & -X & 0 & 0 \\ 0 & 1 & 0 & 0 \end{bmatrix} X(t) + \begin{bmatrix} 1 & 0 & 0 & 0 \\ 0 & 1 & 0 & 0 \\ 0 & 0 & 1 & 0 \\ 0 & 0 & 0 & 1 \end{bmatrix} U(t), \tag{13}$$

where

$$X(t) = [x, y, z, w]^T \quad \text{and}$$
$$U(t) = [u_1, u_2, u_3 + E, u_4]^T.$$

Next, we calculate the minimum and maximum (MM) values of $X(t)$ under $y(t) \in [-2, 2]$, and obtain $\min_{y(t)} X(t) = -2$, $\max_{y(t)} X(t) = 2$. Then, the membership function can be set as

$$h_1(X(t)) = \frac{X(t) + 2}{4}, \quad -2 \le X(t) \le 2,$$
$$h_2(X(t)) = 1 - h_1(X(t)) = \frac{-X(t) + 2}{4}.$$

With MM value, $X(t)$ can be represented by

$$X(t) = x_1(t) = h_1(X(t)) \times (-2) + h_2(X(t)) \times 2.$$

Thus, the systems (14) can be portrayed by the following fuzzy T–S model

$$\dot{X}(t) = \sum_{i=1}^{2} h_i(X(t))[A_i X(t) + B_i U(t)], \quad (14)$$

where

$$A_1 = \begin{bmatrix} -1 & 1 & 0 & 0 \\ -1 & 0.3 & -2 & 0 \\ 0 & 2 & 0 & 0 \\ 0 & 1 & 0 & 0 \end{bmatrix},$$

$$A_2 = \begin{bmatrix} -1 & 1 & 0 & 0 \\ -1 & 0.6 & 2 & 0 \\ 0 & -2 & 0 & 0 \\ 0 & 1 & 0 & 0 \end{bmatrix},$$

$$B_1 = B_2 = \begin{bmatrix} 1 & 0 & 0 & 0 \\ 0 & 1 & 0 & 0 \\ 0 & 0 & 1 & 0 \\ 0 & 0 & 0 & 1 \end{bmatrix}.$$

Consider the zero-order control input. The following is how this concept might be represented in terms of control with time-varying delay:

$$U(t) = U_d(t_k) = U_d(t - (t - t_k)) = U_d(t - h(t)),$$
$$t - t_k = h(t), \ \ t_k \le t < t_{k+1}. \quad (15)$$

The control system under consideration uses a discrete-time control signal U_d and a time-varying delay $h(t) = t - t_k$, where t_k denotes the instant of sampling, satisfying $0 < t_1 < t_2 < \cdots < t_k < \cdots$. The delay function is piecewise linear, with a derivative of $\dot{h}(t) = 1$ for $t \neq t_k$. To better understand the system, we define the sampling interval $h_k = t_{k+1} - t_k$, which is the time between two consecutive sampling instants.

It is important to note that the sampling interval h_k satisfies the inequality $h(t) \le h_k \le h$, for all t. Here, h is the maximum upper bound among all h_k. In other words, the sampling interval h_k is always bounded by the maximum allowable delay h and the current delay at time t, $h(t)$.

Given this setup, we can now define the rules for the controller

$$U(t) = \sum_{j=1}^{2} h_j(X(t_k)) K_j X(t_k). \quad (16)$$

In control systems, a piecewise control law can be represented as a continuous-time control with a time-varying piecewise continuous delay. The delay function, denoted by $h(t)$, is continuous from the right and can be expressed as $h(t) = t - t_k$ according to Eq. (15). To design such a controller, we aim to develop a state-feedback controller that takes the form of a continuous function, which uses information about the current state of the system to compute the appropriate control action

$$U(t) = \sum_{j=1}^{2} h_j(X(t_k)) K_j X(t - h(t)). \quad (17)$$

The closed-loop system (14) with (17) is given by

$$\dot{X}(t) = \sum_{i=1}^{2} \sum_{j=1}^{2} h_i(X(t)) h_j(X(t_k)) \times [A_i X(t) + B_i K_j X(t - h(t))]. \quad (18)$$

The subsequent lemmas are helpful in providing proof for our key conclusions.

Lemma 1. *Let $\mathbb{M} \in \mathbb{R}^{n \times n}$ be a constant symmetric matrix such that $\mathbb{M} = \mathbb{M}^* > 0$. Suppose $\epsilon > 0$ and $z : [0, \epsilon] \to \mathbb{C}^n$ is a vector function. Then,*

$$\left[\int_0^\epsilon z(s)ds\right]^T \mathbb{M}\left[\int_0^\epsilon z(s)ds\right] \le \epsilon \int_0^\epsilon z^T(s)\mathbb{M}z(s)ds.$$

Lemma 2. *Let $\mathcal{D} \subseteq \mathbb{R}^m$ be a set such that $f_1 > 0$, $f_2 > 0, \ldots, f_N > 0 : \mathbb{R}^m \mapsto \mathbb{R}$ are functions that*

take values in $\mathcal{D}$. Then, the reciprocally convex combination of f_i over $\mathcal{D}$ is satisfied

$$\min_{\{\alpha_i \,|\, \alpha_i>0, \sum_i \alpha_i=1\}} \sum_i \frac{1}{\alpha_i} f_i(t) = \sum_i f_i(t) + \max_{g_{ij}(t)} \sum_{i\neq j} g_{i,j}(t)$$

with

$$\left\{ g_{ij} : \mathbb{R}^m \mapsto \mathbb{R}, g_{ij}(t) \triangleq g_{ij}(t), \begin{bmatrix} f_i(t) & g_{ij}(t) \\ g_{ij}(t) & f_j(t) \end{bmatrix} \geq 0 \right\}.$$

4.1. *Main results*

In this section, the sampled-data approach is used to conduct an investigation of the stabilization challenge of the proposed fuzzy system (18).

Theorem 1. *For known scalars $h > 0$ and given K_i, the system (18) is asymptotically stable if there exist matrices $P \in \mathbb{R}^{n\times n} > 0$, $Q \in \mathbb{R}^{n\times n} > 0$, $R \in \mathbb{R}^{n\times n} > 0$, nonsingular matrix Y, any matrices N, positive semi-definite matrices X_{1n}, $n = 1, 2, 3$, X_{22}, X_{23}, X_{33} and satisfying the following LMIs*:

$$\begin{bmatrix} X_{11} & X_{12} & X_{13} \\ * & X_{22} & X_{23} \\ * & * & X_{33} \end{bmatrix} \geq 0, \tag{19}$$

$$\begin{bmatrix} R - X_{33} & N \\ \star & R - X_{33} \end{bmatrix} \geq 0, \tag{20}$$

$$[\Sigma]_{4\times 4} < 0, \tag{21}$$

where

$$\Sigma_{11} = Q - [R - X_{33}] + YA_i + hX_{11} + 2X_{13},$$
$$\Sigma_{12} = P - Y + (YA_i)^T,$$
$$\Sigma_{13} = -Q + N,$$
$$\Sigma_{14} = [R - X_{33}] - N^T + YB_iK_j + hX_{12} - X_{13} + X_{23}^T,$$
$$\Sigma_{22} = h^2[R - X_{33}] - Y,$$
$$\Sigma_{23} = -[R - X_{33}],$$
$$\Sigma_{24} = YB_iK_j,$$
$$\Sigma_{33} = -[R - X_{33}],$$
$$\Sigma_{34} = [R - X_{33}] - N,$$
$$\Sigma_{44} = -2[R - X_{33}] + 2N + hX_{22} - 2X_{23}.$$

Proof. Construct the following LKF:

$$V(X_t, t) = \sum_{i=1}^{3} V_i(X_t, t), \tag{22}$$

where

$$V_1(X_t, t) = X^T(t)PX(t),$$
$$V_2(X_t, t) = \int_{t-h}^{t} X^T(s)QX(s)ds,$$
$$V_3(X_t, t) = h\int_{-h}^{0}\int_{t+\theta}^{t} \dot{X}^T(s)R\dot{X}(s)dsd\theta.$$

Taking the derivative of LKF in (22), we have

$$\dot{V}_1(X_t, t) = 2X^T(t)P\dot{X}(t), \tag{23}$$
$$\dot{V}_2(X_t, t) = X^T(t)QX(t) - X^T(t-h)QX(t-h), \tag{24}$$
$$\dot{V}_3(X_t, t) = \dot{X}^T(t)[h^2R]\dot{X}(t) - h\int_{t-h}^{t} \dot{X}^T(s)R\dot{X}(s)ds. \tag{25}$$

Here,

$$-h\int_{t-h}^{t} \dot{X}^T(s)R\dot{X}(s)ds = -h\int_{t-h}^{t} \dot{X}^T(s)[R - X_{33}]\dot{X}(s)ds - h\int_{t-h}^{t} \dot{X}^T(s)X_{33}\dot{X}(s)ds.$$

Applying Lemmas 1 and 2, $\dot{V}_3(X_t, t)$ yields

$$-h\int_{t-h}^{t} \dot{X}^T(s)[R - X_{33}]\dot{X}(s)ds = -h\int_{t-h}^{t-h(t)} \dot{X}^T(s)[R - X_{33}]\dot{X}(s)ds - h\int_{t-h(t)}^{t} \dot{X}^T(s)[R - X_{33}]\dot{X}(s)ds$$

$$\leq \frac{h}{h-h(t)}\left(\int_{t-h}^{t-h(t)} \dot{X}(s)ds\right)^T [R-X_{33}]\left(\int_{t-h}^{t-h(t)} \dot{X}(s)ds\right)$$
$$-\frac{h}{h(t)}\left(\int_{t-h(t)}^{t} \dot{X}(s)ds\right)^T [R-X_{33}]\left(\int_{t-h(t)}^{t} \dot{X}(s)ds\right)$$
$$\leq -[X(t-h(t))-X(t-h)]^T[R-X_{33}][X(t-h(t))-X(t-h)]$$
$$-[X(t)-X(t-h(t))]^T[R-X_{33}][X(t)-X(t-h(t))]$$
$$-2[X(t)-X(t-h(t))]^T N[X(t-h(t))-X(t-h)]$$
$$= \begin{bmatrix} X(t) \\ X(t-h) \\ X(t-h(t)) \end{bmatrix}^T \begin{bmatrix} -[R-X_{33}] & N & [R-X_{33}]-N^T \\ \star & -[R-X_{33}] & [R-X_{33}]-N \\ \star & \star & -2[R-X_{33}]+N+N^T \end{bmatrix} \begin{bmatrix} X(t) \\ X(t-h) \\ X(t-h(t)) \end{bmatrix}. \quad (26)$$

By using the Leibniz–Newton formula, we obtain the following

$$-\int_{t-h(t)}^{t} \dot{X}^T(s)X_{33}\dot{X}(s)ds \leq \int_{t-h(t)}^{t} \begin{bmatrix} X(t) \\ X(t-h(t)) \\ \dot{X}(s) \end{bmatrix}^T \begin{bmatrix} X_{11} & X_{12} & X_{13} \\ * & X_{22} & X_{23} \\ * & * & 0 \end{bmatrix} \begin{bmatrix} X(t) \\ X(t-h(t)) \\ \dot{X}(s) \end{bmatrix} ds$$
$$\leq X^T(t)(hX_{11}+X_{13}+X_{13}^T)X(t)+2X^T(t)(hX_{12}-X_{13}+X_{23}^T)X(t-h(t))$$
$$+X^T(t-h(t))(hX_{22}-X_{23}-X_{23}^T)X(t-h(t)). \quad (27)$$

Conversely, in the case of a nonsingular matrix Y with dimensions that are appropriate, we get

$$0 = 2[X^T(t)+\dot{X}^T(t)]Y[-\dot{X}(t)+\dot{X}(t)]$$
$$= 2[X^T(t)+\dot{X}^T(t)]Y$$
$$\times\left[-\dot{X}(t)+\sum_{i=1}^{2}\sum_{i=1}^{2} h_ih_j[A_iX(t) + B_iK_jX(t-h(t))]\right]. \quad (28)$$

Now, combining (23)–(28), we get

$$\dot{V}(X_t,t) \leq \zeta^T(t)\Sigma\zeta(t), \quad (29)$$

where,

$$\zeta^T(t) = [x^T(t) \quad \dot{x}(t) \quad x^T(t-h) \quad x^T(t-h(t))].$$

Clearly, the inequality $\Sigma < 0$ implies that $\dot{V}(X_t, t) < 0$, and by applying the Lyapunov–Krasovskii stability theorem, it follows that the system (18) is asymptotically stable. This serves as the concluding step in the proof. ■

Theorem 2. *For known scalars $h > 0$ and the system (18) is asymptotically stable if there exist matrices $\hat{P} > 0 \in \mathbb{R}^{n\times n}$, $\hat{Q} > 0 \in \mathbb{R}^{n\times n}$, $\hat{R} > 0 \in \mathbb{R}^{n\times n}$, nonsingular matrix Y, any matrices $\hat{N}$, L_j, positive semi-definite matrices $\hat{X}_{1n}$, $n = 1, 2, 3$, $\hat{X}_{22}$, $\hat{X}_{23}$, $\hat{X}_{33}$ and satisfying the following LMIs*:

$$\mho_1 \geq 0, \quad (30)$$
$$\mho_2 \geq 0, \quad (31)$$
$$[\Pi]_{4\times 4} < 0, \quad (32)$$

where

$$\Sigma_{11} = \hat{Q} - [\hat{R}-\hat{X}_{33}] + A_i\hat{Y} + h\hat{X}_{11} + 2\hat{X}_{13},$$
$$\Sigma_{12} = \hat{P} - \hat{Y} + (A_i\hat{Y})^T, \quad \Sigma_{13} = -\hat{Q} + \hat{N},$$
$$\Sigma_{14} = [\hat{R}-\hat{X}_{33}] - \hat{N}^T + B_iL_j + h\hat{X}_{12} - \hat{X}_{13} + \hat{X}_{23}^T,$$
$$\Sigma_{22} = h^2[\hat{R}-\hat{X}_{33}] - \hat{Y},$$
$$\Sigma_{23} = -[\hat{R}-\hat{X}_{33}], \quad \Sigma_{24} = B_iL_j,$$

$$\Sigma_{33} = -[\hat{R} - \hat{X}_{33}], \quad \Sigma_{34} = [\hat{R} - \hat{X}_{33}] - N,$$

$$\Sigma_{44} = -2[\hat{R} - \hat{X}_{33}] + 2\hat{N} + h\hat{X}_{22} - \hat{X}_{23} - \hat{X}_{23}^T.$$

Furthermore, the controller gain may be built as $K_j = L_j\hat{Y}^{-1}$.

Proof. Define $\hat{Y} = Y^{-1}$, $\hat{P} = \hat{Y}P\hat{Y}$, $\hat{Q} = \hat{Y}Q\hat{Y}$, $\hat{R} = \hat{Y}R\hat{Y}$, $\hat{N} = \hat{Y}N\hat{Y}$ and

$$\mho_1 = \hat{Y} \otimes \begin{bmatrix} X_{11} & X_{12} & X_{13} \\ * & X_{22} & X_{23} \\ * & * & X_{33} \end{bmatrix} \otimes \hat{Y},$$

$$\mho_2 = \hat{Y} \otimes \begin{bmatrix} [R - X_{33}] & N \\ \star & [R - X_{33}] \end{bmatrix} \otimes \hat{Y} \geq 0.$$

When pre- and post-multiplying (21) with $\text{diag}\{\hat{Y}, \hat{Y}, \hat{Y}, \hat{Y}\}$, we obtain LMIs (32). ■

Remark 4.1. The fuzzy sampled-data stabilization of memristor-based hidden dynamical systems refers to the control technique used to stabilize the behavior of dynamic systems that include memristors, which are a type of electronic component. In this technique, the system is stabilized by using fuzzy logic and sample data, which allows for more robust and adaptive control compared to traditional control methods. The goal is to maintain the desired behavior of the system, even in the presence of uncertainties or disturbances, by making use of the unique properties of memristors.

5. Experimental Results

This section shows, a hardware design of an analog circuit in real-time implementation for the memristor-based hidden system. The circuits verify the extreme events of numerically obtained results of Eq. (6). The schematic circuit and photograph of the breadboard circuit are as shown in Figs. 9(a)–9(c). The entire circuit (Fig. 9) unit operates with ±12 V dual volt power supply. We used Agilent dual volt power supply and utilized the trivial TL082 Op-Amp IC to construct the circuit. In this circuit, the analog multiplier (AD633JN) (M_1, M_2) is used for generating a nonlinear mixture of state variables. The gains of analog multipliers M_1 and M_2 are set as (1/10) V. In real-time experiments, only the two resistors R_4 and R_8 in the hardware analog circuit can be tuned as a control parameter. The memristor symbol is drawn and the subcircuit (Fig. 1) is discussed in the more earlier section of this manuscript. The circuit results were obtained by a digital storage oscilloscope (Agilent InfiniiVision MSO6014A series) at the nodes of capacitors C_1, C_2, C_3 and C_4 respectively. The corresponding circuit equations are written as,

$$\begin{cases} \dfrac{dv_1}{dt} = -\dfrac{1}{R_2C_1}v_1 + \dfrac{1}{R_1C_1}v_2, \\ \dfrac{dv_2}{dt} = -\dfrac{1}{R_3C_2}v_1 + \dfrac{1}{10R_4C_2}v_2v_3 + \dfrac{1}{W(w)C_2}v_2, \\ \dfrac{dv_3}{dt} = \dfrac{1}{R_8C_3}E - \dfrac{1}{10R_7C_3}v_2^2, \\ \dfrac{dv_4}{dt} = \dfrac{1}{R_8C_4}v_2. \end{cases} \tag{33}$$

Here we consider, $v_1 = x$, $v_2 = y$, $v_3 = z$ and v_4 or $\phi = w$. The circuit variables v_1, v_2, v_3 and v_4 are voltages developed across the capacitors C_1, C_2, C_3 and C_4. The time scale transformation $\tau = \tau_0 t$ (physical time constant) on Eq. (6), where $\tau_0 = \text{RC}$ (integral time constant) is the timescale transformation factor and then redefine τ as t. One gets the normalized equations after time scale transformation can be obtained as Eq. (6) which is equivalent to the system parameters being normalized by the following set of circuit equations,

$$\frac{1}{R_1C_1} = \frac{1}{R_2C_1} = 1,$$

$$\frac{1}{W(w)C_2} = \frac{1}{R_3C_2} = \frac{1}{10R_4C_2} = 1,$$

$$\frac{1}{R_8C_3} = \frac{1}{10R_7C_2} = 1,$$

$$\frac{1}{RC} = 1.$$

The time-constant related circuit elements are optimized as $R = 10\,\text{k}\Omega$ and $C = 4.7\,\text{nF}$. Other circuit elements values are calculated and fixed as $C_1 = C_2 = C_3 = C_4 = 4.7\,\text{nF}$, R_1, R_2, R_3, R_5, $R_6 = 10\,\text{k}\Omega$, $R_4 = 4.7\,\text{k}\Omega$, $R_7 = 100\,\text{k}\Omega$ and for the real-time experimental study, we use the resistor R_8, for varying the external bias E as a control parameter using a tunable potentiometer (100 kΩ). Notice that the circuit components are ±5% tolerances.

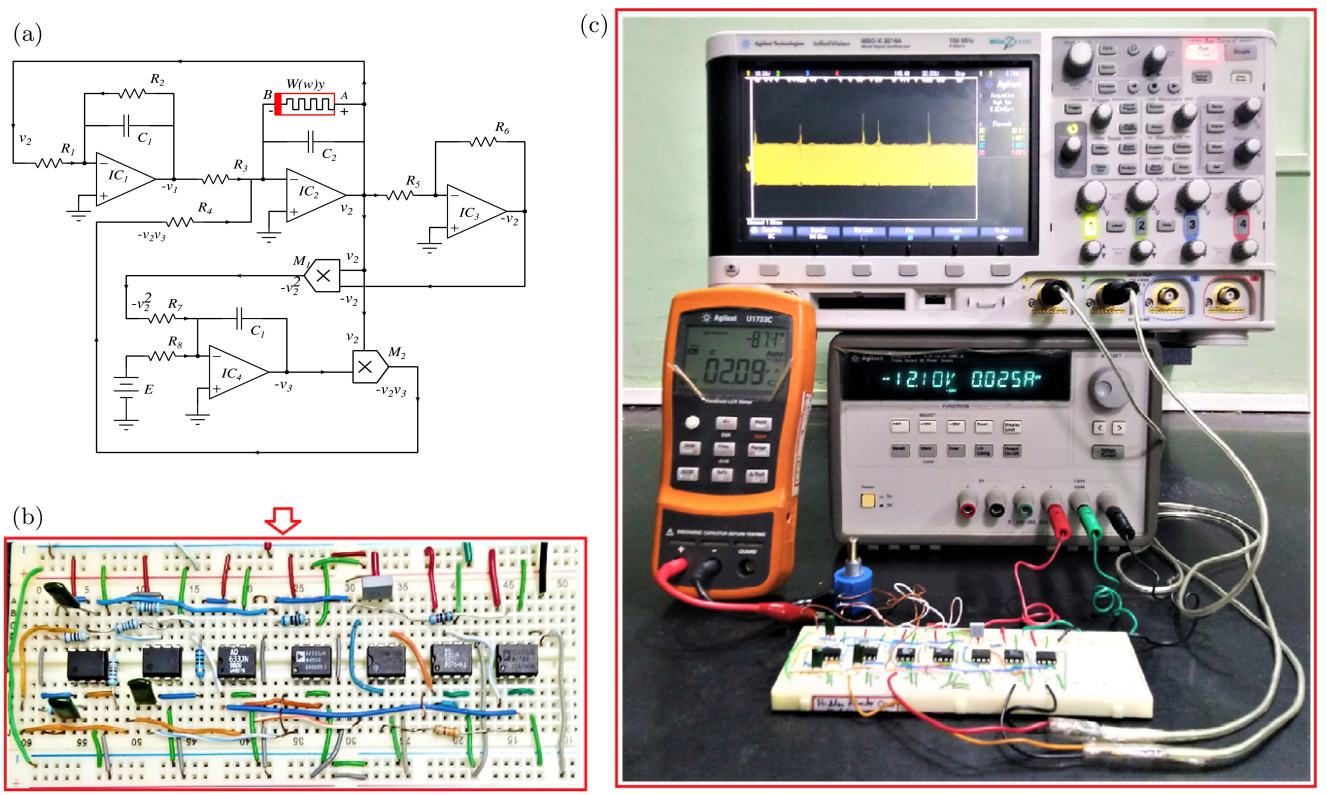

Fig. 9. (a) Schematic circuit diagram of the proposed memristor-based system, (b) photograph of a real-time analog circuit configured on a breadboard and (c) entire experimental setup.

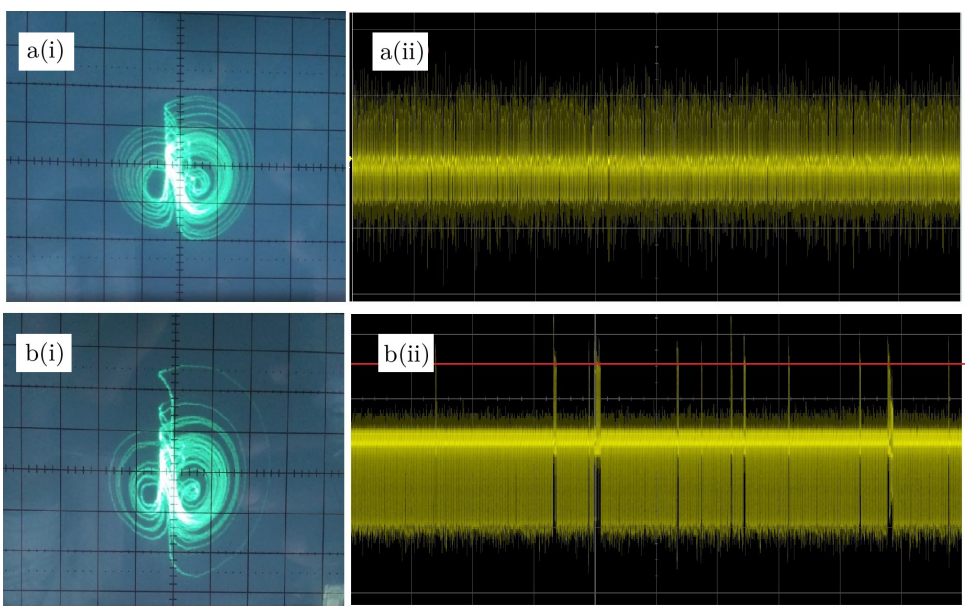

Fig. 10. Experimentally obtained (a) typical bounded chaotic attractor and (b) extreme events oscillations. (i) Phase portraits in the (v_{C_1}–v_{C_2}) planes and (ii) time series ($v_{C_2}(t)$), (*horizontal*-axis 100 mV/div, *vertical*-axis 25 mA/div).

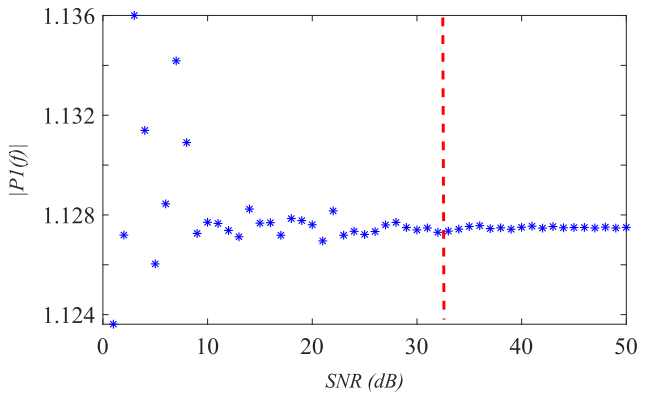

Fig. 11. Numerically computed frequency component $|P1(f)|$ as a function of SNR for the experimental time series data of $(v_{c2}(t))$ mixed with Gaussian noise.

5.1. *Experimental observations*

For obtaining the experimental results, the potentiometer R_8 gives (the variation in external bias E) the dynamics of the system. The synopsis of the results are,

- For $R_8 = 0\,\Omega$: Fixed point.
- For $43\,\text{k}\Omega < R_8 \leq 50\,\text{k}\Omega$: Period-doubling sequence.
- For $54\,\text{k}\Omega < R_8 \leq 72\,\text{k}\Omega$: Chaotic regime.
- For $76\,\text{k}\Omega < R_8 \leq 94\,\text{k}\Omega$: Extreme Events regime.

For visualizing the experimental results, Fig. 10(a) shows the chaotic oscillations at $R_8 = 69\,\text{k}\Omega$ and Fig. 10(b) shows the extreme event oscillations at

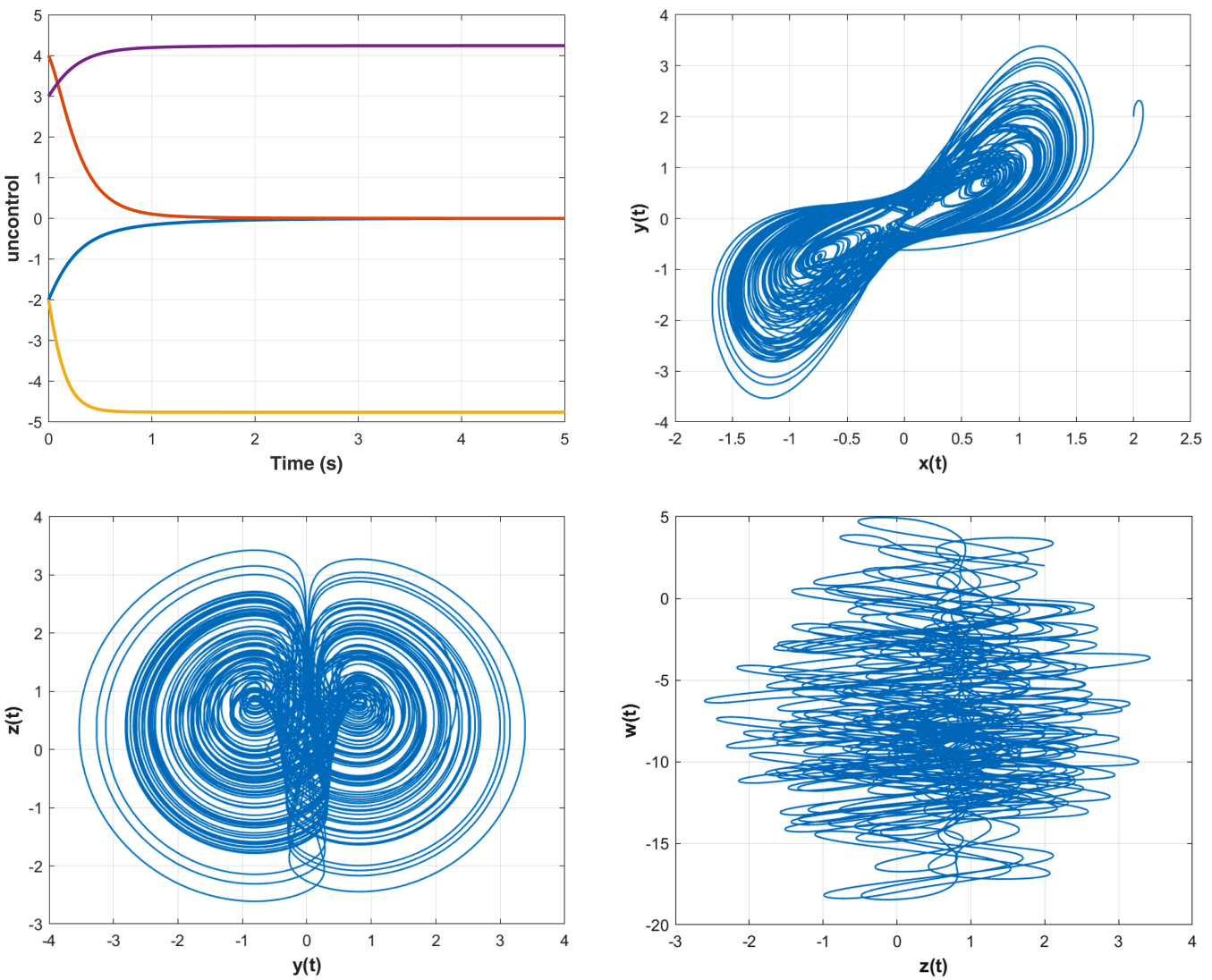

Fig. 12. Extreme events hidden with memristor oscillator without control response.

$R_8 = 84\,\text{k}\Omega$. The phase portraits in the (i) (v_{C_1}–v_{C_2}) plane and its corresponding (ii) time evolution's $v_{C_2}(t)$ circuit state variables are plotted. Through the calculation of extreme events from experimentally obtained time series data, we found, $\mu = 0.3422\,\text{mV}$ and $\sigma = 0.3231\,\text{mV}$, and EE = $2.2811\,\text{mV}$. The horizontal red line represents the EE threshold for demonstration.

5.2. *Signal-to-noise ratio* (*SNR*)

To confirm the noise level of obtained signals from the circuit, a signal-to-noise ratio (SNR = $\frac{P_{\text{signal}}}{P_{\text{noise}}}$) analysis calculation is performed. The power of signal and noise are calculated from power spectrum analysis. Our data has SNR = 33 dB, which confirms the signal is robust against noise. Figure 11 shows SNR values with respect to the frequency component of the data/signal. In the x-axis, we have added to this time series Gaussian noise of various amplitudes ranging from 1 dB to 100 dB. When the noise levels are very high (that is, for SNR $< 33\,\text{dB}$), we find that the spectrum is scattered, while for substantial noise levels (that is, for SNR $\geq 33\,\text{dB}$), the spectrum is regular. In Fig. 11, the vertical red dashed line shows the demarcation of the effect of noise on the time series for $v_{c2}(t)$. This shows that the experimental data are robust even up to 73% of the noise levels.

6. Simulation Results

In addition, using LMI (30)–(32) in Theorem 2 with a sampling time of $h = 0.12$ and the MATLAB LMI Control Toolbox, the following control gains were obtained:

$$K_1 = [0.0758 \quad -1.0024 \quad 1.0350 \quad -0.1124] \quad \text{and}$$

$$K_2 = [-0.0758 \quad 1.0024 \quad -1.0350 \quad 0.1124].$$

Figure 12 depicts the system state reaction when there is no control input, and Fig. 13 shows the system state response when there is a control input. It is straightforward to see that the system arrives at a stable state over time, which demonstrates that the suggested controller is both reliable and effective in its execution.

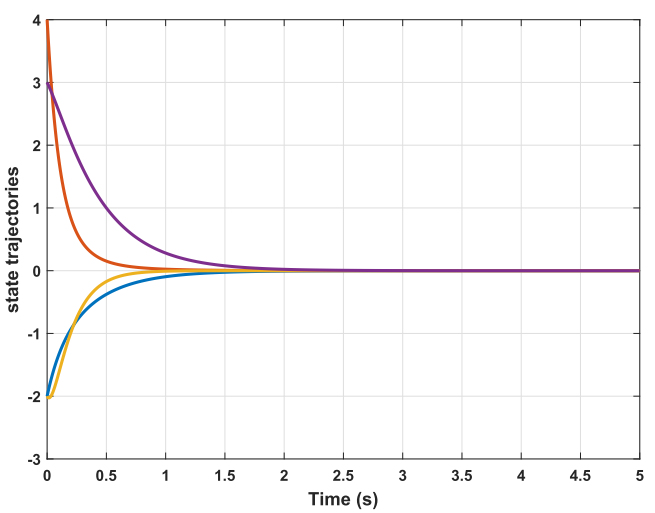

Fig. 13. State response of the extreme events hidden with memristor oscillator with control.

7. Conclusions

For the first time, we studied the occurrence of extreme events and hidden attractors on the memristor-based four-dimensional system numerically and experimentally in this manuscript. The hidden oscillations as well as the cause of the oscillations are confirmed by stability analysis. Furthermore, the extreme events were discovered and confirmed in a set of external biasing parameters. The existence of extreme events (EEs) proved conclusively using numerical and statistical calculations such as the probability distribution function (PDF) and phase slip graphs. The designed real-time hardware experimental circuit and the experimental results match the numerically simulated extreme events. To understand the period-doubling scenario, we also computed the bifurcation diagram and its corresponding Lyapunov spectra.

In the second phase of the manuscript, the control mechanism is applied to control the phenomenon of extreme events. In order to find the stabilization of the proposed model, we handle the sampled data control scheme. By constructing a suitable Lyapunov function and using superior inequality techniques, the asymptotic stability of the addressed model is established in terms of LMIs. Moreover, the corresponding sampled-data controller can be synthesized by solving a set of LMIs, which can be solved by the MATLAB LMI toolbox, under the premise of obtaining the optimal parameters and the maximum sampling interval.

We hope that the results of our current work will be extended to the coupled network of oscillators and the design of the controller using an event-triggered scheme in the future to save network resources. We are already well into this, and the results will be presented in subsequent articles.

The current paper improves our understanding of the dynamics of memristor-based dynamical systems. The results are promising, and they are applicable to the development of the memristor emulator and circuit theory. Furthermore, the controlling EEs and hidden oscillations suggest a method for stabilizing memristor systems. In the future, we intend to investigate the impact of controlling and the evolution of hidden and extreme events in a coupled network of system configurations.

Acknowledgments

K. Thamilmaran acknowledges Chennai Institute of Technology for the experimental and computational assistance. S. Sabarathinam and V. Popov acknowledge the Basic Research Program of the National Research University, Higher School of Economics, Moscow.

Conflict of Interest

The authors declare that they have no conflict of interest.

Data Availability

The data that support the findings of this study are available from the corresponding author upon request.

References

Ackermann, J. [2012] *Sampled-Data Control Systems*: *Analysis and Synthesis*, *Robust System Design* (Springer Science & Business Media).

Anbuvithya, R., Sri, S. D., Vadivel, R., Gunasekaran, N. & Hammachukiattikul, P. [2021] "Extended dissipativity and non-fragile synchronization for recurrent neural networks with multiple time-varying delays via sampled-data control," *IEEE Access* **9**, 31454–31466.

Andrievsky, B., Kravchuk, K., Kuznetsov, N. V., Kuznetsova, O. A. & Leonov, G. A. [2016] "Hidden oscillations in the closed-loop aircraft-pilot system and their prevention," *IFAC-PapersOnLine* **49**, 30–35.

Bao, B., Bao, H., Wang, N., Chen, M. & Xu, Q. [2017] "Hidden extreme multistability in memristive hyperchaotic system," *Chaos Solit. Fract.* **94**, 102.

Burr, G. W., Shelby, R. M., Sebastian, A., Kim, S., Kim, S., Sidler, S., Virwani, K., Ishii, M., Narayanan, P., Fumarola, A. *et al.* [2017] "Neuromorphic computing using non-volatile memory," *Adv. Phys.*: *X* **2**, 89.

Chaurasia, S. S., Verma, U. K. & Sinha, S. [2020] "Advent of extreme events in predator populations," *Scient. Rep.* **10**, 1.

Chua, L. [1971] "Memristor — The missing circuit element," *IEEE Trans. Circuit Th.* **18**, 507.

Corinto, F. & Forti, M. [2016] "Memristor circuits: Flux-charge analysis method," *IEEE Trans. Circuits Syst.-I*: *Regular Papers* **63**, 1997–2009.

Danca, M.-F. [2021] "Coexisting hidden and self-excited attractors in an economic model of integer or fractional order," *Int. J. Bifurcation and Chaos* **31**, 2150062-1–15.

Ding, K. & Zhu, Q. [2020] "A note on sampled-data synchronization of memristor networks subject to actuator failures and two different activations," *IEEE Trans. Circuits Syst.-II*: *Express Briefs* **68**, 2097–2101.

Dudkowski, D., Jafari, S., Kapitaniak, T., Kuznetsov, N. V., Leonov, G. A. & Prasad, A. [2016] "Hidden attractors in dynamical systems," *Phys. Rep.* **637**, 1–50.

Gunasekaran, N. & Joo, Y. H. [2019] "Stochastic sampled-data controller for T–S fuzzy chaotic systems and its applications," *IET Contr. Th. Appl.* **13**, 1834.

Gunasekaran, N., Srinivasan, S., Zhai, G. & Yu, Q. [2021a] "Dynamical analysis and sampled-data stabilization of memristor-based Chua's circuits," *IEEE Access* **9**, 25648–25658.

Gunasekaran, N., Zhai, G. & Yu, Q. [2021b] "Exponential sampled-data fuzzy stabilization of nonlinear systems and its application to basic buck converters," *IET Contr. Th. Appl.* **15**, 1157–1168.

Haghiri, S., Nemati, A., Feizi, S., Amirsoleimani, A., Ahmadi, A. & Ahmadi, M. [2017] "A memristor based binary multiplier," *2017 IEEE 30th Canadian Conf. Electrical and Computer Engineering* (*CCECE*) (IEEE), pp. 1–4.

Hamdioui, S., Taouil, M. & Haron, N. Z. [2013] "Testing open defects in memristor-based memories," *IEEE Trans. Comput.* **64**, 247–259.

Hu, X., Liu, C., Liu, L., Ni, J. & Li, S. [2016] "Multi-scroll hidden attractors in improved Sprott A system," *Nonlin. Dyn.* **86**, 1725–1734.

Jafari, S., Sprott, J. & Nazarimehr, F. [2015] "Recent new examples of hidden attractors," *The Europ. Phys. J. Special Topics* **224**, 1469–1476.

Jafari, S., Ahmadi, A., Khalaf, A. J. M., Abdolmohammadi, H. R., Pham, V.-T. & Alsaadi, F. E. [2018] "A new hidden chaotic attractor with extreme multistability," *AEU — Int. J. Electron. Commun.* **89**, 131–135.

Jothimurugan, R., Sabarathinam, S., Suresh, K. & Thamilmaran, K. [2017] "Experimental analogue implementation of memristor based chaotic oscillators," *Advances in Memristors*, *Memristive Devices and Systems*, pp. 343–370.

Kahale, T. & Tannir, D. [2021] "Memristor modeling using the modified nodal analysis approach," *IEEE Trans. Comput.-Aided Design Integrated Circuits Syst.* **41**, 1191–1195.

Kim, H., Sah, M. P., Yang, C., Cho, S. & Chua, L. O. [2012] "Memristor emulator for memristor circuit applications," *IEEE Trans. Circuits Syst.-I*: *Regular Papers* **59**, 2422–2431.

Kirezci, E., Young, I. R., Ranasinghe, R., Muis, S., Nicholls, R. J., Lincke, D. & Hinkel, J. [2020] "Projections of global-scale extreme sea levels and resulting episodic coastal flooding over the 21st century," *Scient. Rep.* **10**, 1.

Kiseleva, M. A., Kuznetsov, N. V. & Leonov, G. A. [2016] "Hidden attractors in electromechanical systems with and without equilibria," *IFAC-PapersOnLine* **49**, 51–55.

Knobler, S., Bar, D., Cohen, R. & Liberzon, D. [2021] "Wave height distributions and rogue waves in the Eastern mediterranean," *J. Marine Sci. Engin.* **9**, 660.

Kumarasamy, S. & Pisarchik, A. N. [2018] "Extreme events in systems with discontinuous boundaries," *Phys. Rev. E* **98**, 032203.

Kuznetsov, A., Kuznetsov, S., Mosekilde, E. & Stankevich, N. [2015] "Co-existing hidden attractors in a radio-physical oscillator system," *J. Phys. A*: *Math. Theoret.* **48**, 125101.

Li, M., Chen, X., Liu, M., Zhang, Y. & Zhang, H. [2020] "Asynchronous adaptive fault-tolerant sliding-mode control for T–S fuzzy singular Markovian jump systems with uncertain transition rates," *IEEE Trans. Cybernet.* **52**, 544–555.

Liu, L., Du, C., Ding, Q., Shi, S., Zhang, S. & Zhang, M. [2020] "Memristive hidden chaotic system and circuit based on Sprott-2 system," *2020 IEEE 3rd Int. Conf. Electronics Technology* (*ICET*) (IEEE), p. 110.

Liu, T., Yan, H., Banerjee, S. & Mou, J. [2021] "A fractional-order chaotic system with hidden attractor and self-excited attractor and its DSP implementation," *Chaos Solit. Fract.* **145**, 110791.

Meilianda, E., Lavigne, F., Pradhan, B., Wassmer, P., Darusman, D. & Dohmen-Janssen, M. [2021] "Barrier islands resilience to extreme events: Do earthquake and Tsunami play a role," *Water* **13**, 178.

Mishra, A., Leo Kingston, S., Hens, C., Kapitaniak, T., Feudel, U. & Dana, S. K. [2020] "Routes to extreme events in dynamical systems: Dynamical and statistical characteristics," *Chaos* **30**, 063114.

Osinga, H. M. & Feudel, U. [2000] "Boundary crisis in quasiperiodically forced systems," *Physica D* **141**, 54.

Pham, V.-T., Vaidyanathan, S., Volos, C. & Kapitaniak, T. [2018] *Nonlinear Dynamical Systems with Self-Excited and Hidden Attractors*, Vol. 133 (Springer).

Poblete, B., Guzmán, J., Maldonado, J. & Tobar, F. [2018] "Robust detection of extreme events using Twitter: Worldwide earthquake monitoring," *IEEE Trans. Multimed.* **20**, 2551.

Premraj, D., Suresh, K., Pawar, S. A., Kabiraj, L., Prasad, A. & Sujith, R. [2021] "Dragon-king extreme events as precursors for catastrophic transition," *EPL* (*Europhys. Lett.*) **134**, 34006.

Sabarathinam, S. & Thamilmaran, K. [2017] "Effect of variable memristor emulator in a Duffing nonlinear oscillator," *AIP Conference Proc.* (AIP Publishing LLC), p. 060007.

Sabarathinam, S. & Prasad, A. [2018] "Memristor emulator causes dissimilarity on a coupled memristive systems," *AIP Conference Proceedings* (AIP Publishing LLC), p. 060025.

Saha, P., Saha, D., Ray, A. & Chowdhury, A. [2015] "Memristive non-linear system and hidden attractor," *The European Phys. J. Special Topics* **224**, 1563–1574.

Sakthivel, R., Karthick, S. A., Wang, C. & Kanakalakshmi, S. [2023] "Finite-time reliable sampled-data control for fractional-order memristive neural networks with quantisation," *J. Exper. Theoret. Artif. Intell.* **35**, 109–127.

Shanmugam, L. & Joo, Y. H. [2020] "Stability and stabilization for T–S fuzzy large-scale interconnected power system with wind farm via sampled-data control," *IEEE Trans. Syst. Man Cybernet.*: *Syst.* **51**, 2134–2144.

Sharma, P., Shrimali, M., Prasad, A., Kuznetsov, N. & Leonov, G. [2015] "Control of multistability in hidden attractors," *The European Phys. J. Special Topics* **224**, 1485–1491.

Shi, K., Wang, J., Zhong, S., Tang, Y. & Cheng, J. [2020] "Non-fragile memory filtering of T–S fuzzy delayed neural networks based on switched fuzzy sampled-data control," *Fuzzy Sets Syst.* **394**, 40–64.

Shin, S., Kim, K. & Kang, S.-M. [2010] "Memristor applications for programmable analog ICs," *IEEE Trans. Nanotechnol.* **10**, 266–274.

Swathy, P., Sabarathinam, S., Suresh, K. & Thamilmaran, K. [2014] "Chaos synchronization and transmission of information in coupled SC-CNN-based canonical Chua's circuit," *Nonlin. Dyn.* **78**, 1033.

Thangavel, B., Srinivasan, S. & Kathamuthu, T. [2021] "Extreme events in a forced BVP oscillator: Experimental and numerical studies," *Chaos Solit. Fract.* **153**, 111569.

Thangavel, B., Srinivasan, S., Kathamuthu, T., Zhai, G. & Gunasekaran, N. [2022] "Dynamical analysis of T–S fuzzy financial systems: A sampled-data control approach," *Int. J. Fuzzy Syst.* **24**, 1–14.

Ueta, T., Miyazaki, H., Kousaka, T. & Kawakami, H. [2004] "Bifurcation and chaos in coupled BVP oscillators," *Int. J. Bifurcation and Chaos* **14**, 1305–1324.

Vadivel, R., Srinivasan, S., Wu, Y. & Gunasekaran, N. [2021] "Study on bifurcation analysis and T–S fuzzy sampled-data stabilization of permanent magnet synchronous motor systems," *Commun. Nonlin. Sci. Numer. Simul.* **125**.

Vadivel, R., Sabarathinam, S., Wu, Y., Chaisena, K. & Gunasekaran, N. [2022] "New results on T–S fuzzy sampled-data stabilization for switched chaotic systems with its applications," *Chaos Solit. Fract.* **164**, 112741.

Varshney, V., Sabarathinam, S., Prasad, A. & Thamilmaran, K. [2018a] "Infinite number of hidden attractors in memristor-based autonomous Duffing oscillator," *Int. J. Bifurcation and Chaos* **28**, 1850013-1–13.

Varshney, V., Sabarathinam, S., Thamilmaran, K., Shrimali, M. & Prasad, A. [2018b] "Existence and control of hidden oscillations in a memristive autonomous Duffing oscillator," *Nonlinear Dynamical Systems with Self-Excited and Hidden Attractors* (Springer, Cham), pp. 327–344.

Wang, X., Park, J. H., Zhong, S. & Yang, H. [2019] "A switched operation approach to sampled-data control stabilization of fuzzy memristive neural networks with time-varying delay," *IEEE Trans. Neural Netw. Learn. Syst.* **31**, 891–900.

Zhai, G. & Xu, X. [2011] "A commutation condition for stability analysis of switched linear descriptor systems," *Nonlin. Anal.*: *Hybrid Syst.* **5**, 383.